BIOCHEMISTRY
including biophysical chemistry & molecular biology

Article

Promotion or Inhibition of IAPP Aggregation by Zinc Coordination Depends on Its Relative Concentration

Praveen Nedumpully-Govindan, Ye Yang, Rachel Andorfer, Weiguo Cao, and Feng Ding

Biochemistry, **Just Accepted Manuscript** • DOI: 10.1021/acs.biochem.5b00891 • Publication Date (Web): 25 Nov 2015

Just Accepted

ACS Publications

Biochemistry is published by the American Chemical Society. 1155 Sixteenth Street N.W., Washington, DC 20036

Promotion or Inhibition of IAPP Aggregation by Zinc Coordination Depends on Its Relative Concentration

Praveen Nedumpully-Govindan, [a] Ye Yang, [b] Rachel Andorfer, [a] Weiguo Cao, [b] and Feng Ding[a,*]

[a]Department of Physics and Astronomy, Clemson University, Clemson, SC 29634
[b]Department of Genetics and Biochemistry, Clemson University, Clemson, SC 29634
[*]Correspondence to Feng Ding: fding@clemson.edu; Tel.: 864-656-0459; Fax: 864-656-0805

Abbreviations:
IAPP, islet amyloid polypeptide
hIAPP, human IAPP
T2D, type-II diabetes
DMD, discrete molecular dynamics
ThT, Thioflavin-T
MW, molecular weight
GWAS, genome wide association study
ZnT8, zinc transporter 8

Abstract

Zinc is reported to play a complex role in islet amyloid polypeptide (IAPP) aggregation, which is associated with β-cell death in type-II diabetes (T2D). Depending on their relative concentrations *in vitro*, zinc could either promote or inhibit IAPP aggregation. Interestingly, genome-wide-association studies suggested both positive and negative correlations between T2D risks and activities of a β-cell-specific zinc transporter upon mutations, which determines zinc concentration *in vivo*. To decipher the effect of zinc coordination on IAPP aggregation, we performed atomistic discrete molecular dynamics simulations to systemically study aggregation propensities of zinc-coordinated IAPP oligomers with different molecular weights (MWs), whose populations are determined by zinc concentration. We find that at low zinc:IAPP stoichiometry, zinc coordination promotes aggregation by forming high-MW oligomers. The aggregation is inhibited when the stoichiometry increases and zinc binds individual peptides. Our computationally derived predictions are validated by complementary Thioflavin-T fluorescence assay measuring the dependence of IAPP aggregation on a wide range of zinc concentrations. Our combined computational and experimental study offers a detailed mechanistic insight into the complex role of zinc on IAPP aggregation and T2D development.

Islet amyloid polypeptide (IAPP), a.k.a. amylin, is a 37-residue peptide whose aggregation is linked to pancreatic β-cell death in type-II diabetes (T2D).[1,2] IAPP is stored together with insulin in β-cell granules before their co-secretion to the blood stream. IAPP has a number of functions, such as delaying gastric emptying to help maintain blood glucose level.[3] Aberrant amyloid aggregates formed by IAPP are found in the pancreas of 90% of T2D patients upon postmortem examination.[4] Experimental studies indicate that IAPP aggregates, including soluble oligomers and/or insoluble fibrils, are toxic to insulin-secreting β-cells.[5] Hence, IAPP aggregation and subsequent β-cell death are believed to cause later-stage insulin deficiency in T2D patients.[6] According to *in vitro* studies, human IAPP (hIAPP) is one of the most amyloidogenic peptides and its aggregation occurs even at low-μM concentrations.[7] However, the peptide is stored at ~mM concentrations inside the β-cell granules;[8] and despite this high concentration, hIAPP aggregation is precluded in the pancreas of non-diabetic individuals. The native inhibition of hIAPP aggregation hinges on specific environmental factors inside the β-cell granules such as the presence of insulin and low pH, which have a known inhibitory effect on hIAPP aggregation.[9–11] While insulin inhibits hIAPP aggregation *in vitro*, it forms a crystal inside the core of β-cell granules,[12] reducing its availability to inhibit hIAPP aggregation *in vivo*.

Another major factor believed to natively inhibit hIAPP aggregation in β-cell granules is a high concentration of zinc ions at mM level, which is actively transported inside by a β-cell specific zinc transporter, ZnT8.[13] According to *in vitro* studies, zinc can either enhance[9] or inhibit[14,15] hIAPP aggregation depending on their relative concentrations. In an early study, the Steiner group reported that adding $ZnCl_2$ to a 250 μM hIAPP solution enhanced the formation of hIAPP aggregation.[9] Such a zinc-induced aggregation enhancement was reduced when 1 mM $ZnCl_2$ was added to the solution. In another recent study of hIAPP aggregation at a lower peptide concentrations (5 and 10 μM), an inhibition of aggregation at "low" concentrations and partial recovery at "high" concentrations of $ZnCl_2$ has also been reported.[14,15] Notably, the lowest concentration of $ZnCl_2$ in this study (~25 μM) was already much higher than the hIAPP concentrations. Interestingly, the complex role of zinc ions on the development of T2D has also been observed at the population level. In an early genome-wide association study (GWAS), mutations in ZnT8 were found to be correlated with T2D risk.[16] An activity-reducing W325R mutation of ZnT8[12] is associated with an increased diabetic risk,[16] suggesting that zinc helps prevent T2D. However, in a recent GWAS study by Flannick *et al*.,[17] a stronger correlation is observed between loss-of-function mutations of ZnT8 and reduced diabetic risk, suggesting that zinc deficiency may be beneficial for reducing T2D. The authors proposed ZnT8 as a potential inhibitor target against T2D. Therefore, in order to determine whether targeting ZnT8 is a truly effective therapeutic approach against T2D, it is necessary to fully understand the complex effect of zinc on hIAPP aggregation and T2D development.

To explain the complex dependence of hIAPP aggregation on zinc concentration observed *in vitro*, a two-site binding mechanism has been proposed[15]. It was suggested that at lower concentrations one zinc ion can bind up to six hIAPP monomers at a high-affinity site (histidine 18, His18), resulting in the formation of an off-pathway oligomer toward amyloid aggregation. But, at higher zinc concentrations, zinc also binds to a secondary low-affinity binding site, which promotes fibril formation. Although this model explains the effect of zinc at the considered concentration range, i.e., inhibition followed by recovery of IAPP aggregation, it cannot explain the other experimentally observed enhancement of IAPP aggregation at relatively

low zinc:hIAPP stoichiometry. Moreover, hIAPP has only one residue, His18,[14] with strong affinity to bind zinc.

In this work, we introduce a simple alternative mechanism to explain the complex effect of zinc binding on hIAPP aggregation. We postulate that zinc can stabilize a number of zinc-coordinated hIAPP oligomers with different molecular weights (MWs), each having a different aggregation propensity. Some of these zinc-coordinated oligomers are aggregation prone (i.e. on-pathway toward amyloid fibrils), but others might be less aggregating (off-pathway). Depending on the relative concentrations of zinc and hIAPP, the population of the oligomers may vary, resulting in different aggregation behavior. To test our hypothesis, we applied all-atom discrete molecular dynamics (DMD) simulations[18,19] to systematically study the structure, dynamics and aggregation propensities of zinc-coordinated hIAPP oligomers with different MWs. DMD is a special type of molecular dynamics algorithm, featuring accurate modeling and rapid sampling of protein conformational dynamics, which enabled us to observe the folding of a set of small proteins to their near-native states[18,19] and protein-peptide recognition.[20] The high computational efficiency of DMD allowed us to reach a cumulative 4.5 μs simulations of zinc-coordinated hIAPP oligomers with different MWs. To validate our computationally derived results, we performed Thioflavin-T (ThT) assay *in vitro* to determine the aggregation of hIAPP under a wide range of zinc concentrations. The experimentally derived dependence of hIAPP aggregation on zinc concentrations confirmed predictions derived from computer simulations. Specifically, at low zinc:hIAPP stoichiometry, zinc coordinates multiple hIAPP to form zinc-bound oligomers, which promotes aggregation with increased local concentration of hIAPP. As the stoichiometry increases and zinc ions bind to individual hIAPP peptides, the aggregation of hIAPP is inhibited due to electrostatic repulsion between the charged zinc ions. The reported slow recovery of aggregation at very high zinc concentration can be explained by the increased screening of electrostatics at high salt concentration. Therefore, our combined experimental and computational study provides a novel mechanistic insight into the complex role of zinc in hIAPP aggregation and T2D development.

Materials and methods

DMD simulations. Simulations were carried out using discrete molecular dynamics (DMD) algorithm.[18,19] DMD makes use of discrete potential functions instead of continuous potentials used in conventional molecular dynamics simulations. During DMD simulations, an atom's velocity remains constant until it encounters a potential step, upon which the velocity is instantaneously changed according to the laws of conservation of energy, momentum and angular momentum. The simulations proceed as a series of such collisions, which can be predicted using sorting algorithms. The use of discrete potential reduces the number of required calculations. Additionally, DMD makes use of an implicit solvent model. Because of these reasons, DMD simulations are faster than conventional molecular dynamics simulations. In the energy function, terms representing bonded, van der Waals, hydrogen bond, solvation and electrostatic interactions are included. Lazaridis-Karplus implicit solvation method[21] was used for representing the solvation and an environment-dependent reaction-like algorithm for hydrogen bonds. The Debye-Hückel approximation was used to model the screened electrostatic interactions. The Debye length of ~10 Å, which corresponds to a physiological salt concentration of 100 mM, and an electric susceptibility of 80 for water was used. As a result, the electrostatic

interactions between charged groups are highly screened in DMD simulations. The temperature in DMD is maintained using the Andersen's thermostat[22].

Modeling zinc-histidine coordination. The binding of zinc with amino acids such as histidine is strong, with disassociation constants varying from micromolar to picomolar range.[23–25] Therefore, we assume that the zinc-His18 coordination bond would not break during the simulation. In order to model the zinc-histidine coordination bond in DMD, we first searched PDB for all structures containing zinc ions, which results in 9547 such cases. The coordination number of zinc varies from two to eight in these structures, and in the most common ones zinc binds to four (tetramer) or six (hexamer) residues. Correspondingly, the coordination spheres have tetrahedral or octahedral geometries. In many cases, zinc ions bind to fewer amino acid residues than required for the full coordination, which may be completed by water molecules. Thus, zinc-coordination enjoys a certain degree of flexibility in terms of the coordination number.

A number of constraint potentials with square well functions (Fig. S2) were assigned to mimic the experimentally observed zinc-histidine binding. The coordination bond was assumed between zinc ions and NE2 atoms. Since the coordination between zinc and imidazole is co-planar, we used additional constraints between zinc ion and all the other four imidazole atoms to ensure planarity. The bond lengths are obtained from the highest peak values of their distribution in 9547 PDB structures (see Fig. S1 and Table S1). Additionally, the geometry of the coordination (i.e., either tetrahedral or octahedral arrangement of NE2 atoms around the central zinc as observed experimentally[23]) was also imposed with the use of a square-well potential restricting the distance between NE2 atoms of different histidines taking part in the coordination bond. The mean NE2-NE2 distance is calculated using the NE2-zinc bond length and the ideal bond angles for tetrahedral (109.7°, for dimers, trimers, and tetramers) or octahedral (90° and 180°, for hexamers) geometries.

Modeling the zinc-bound hIAPP oligomers. The hIAPP coordinates were obtained from the protein data bank (PDB ID: 2L86).[26] The initial structures were prepared by hand using PyMol (http://www.pymol.org) by placing the hIAPP chains around the zinc ion with His18 (NE2 atoms) close to the zinc ion, similar to the ideal coordination bond. For trimers and higher oligomers, steric clashes hampered placement of hIAPP chains close to each other. To circumvent this issue, we placed the chains farther apart and used a weak attractive potential between zinc and NE2 atoms and a short simulation of 0.5 ns was carried out at a low temperature (275K), to ensure that the coordinated initial structures are formed. Once the coordination bonds were relaxed, each imidazole could freely rotate around the zinc-NE2 bond, allowing the zinc-coordinated hIAPP oligomer to relax from the initial condition. To avoid any bias arising from the initial structure, different initial structures with randomly chosen orientations were constructed for each of the independent simulations.

Simulation setup. Since we were interested in both the thermodynamics and kinetics of aggregation, we performed constant temperature simulations at 300K instead of using enhanced sampling methods like replica exchange, where the derivation of kinetics information from simulations is not straightforward. To achieve sufficient sampling, ten independent runs were carried out for each molecular system. The initial relative orientations of monomers and the

initial velocities were randomly chosen for each independent run. Each simulation is carried out for one million steps or 50 ns. The values reported were averaged over the last half of the simulations unless stated otherwise. The simulations were carried out in cubic boxes of size 100 (monomer), 120 (dimer), 200 (trimer) or 300 Å (tetramer and hexamer).

Contact number and hydrogen bond calculation. The amyloidogenic contact number was obtained by calculating the number of atomic contacts between each pair of chains, and dividing the sum over all pairs by the number of chains. A contact was defined if the distance between two heavy atoms is less than 6.5Å. Only residues 22–29 was considered for this calculation. A similar approach was used for the calculation of hydrogen bonds. The total number of hydrogen bonds formed by the backbone atoms was calculated. Two residues were defined to make hydrogen bond if the distance between proton and acceptor, $d_{HA} < 2.5$Å and the angles $\theta_{DHA} > 90°$ and $\theta_{HAX} > 90°$. Only residues 22–29 were considered for hydrogen bond calculation as well.

Thioflavin-T Fluorescence Assay. To study the kinetics of hIAPP amyloid fibril formation *in vitro*, human-IAPP (KCNTATCATQRLANFLVHSSNNFGAILSSTNVGSNTY-NH_2), with a Cys2-Cys7 disulfide bridge, was synthesized commercially (California Peptide Research) and its purity verified by reverse phase HPLC. After lyophilization, ~1 mg hIAPP was first solubilized in 100% hexafluorosiopropanol (HFIP) (Sigma) at ~1 mM as stock. The concentration was determined spectrophotometrically using a calculated extinction coefficient at 280 nm of 2000 $M^{-1}cm^{-1}$. To initiate fiber formation, the hIAPP stock was diluted to a final concentration of 10 μM in 100 mM Tris-HCl (pH 7.5), 100 mM NaCl, 25 μM ThT (Sigma) and varying concentrations of $ZnCl_2$. All buffers were passed through HiTrap Chelating HP Column (GE Healthcare) to remove trace amount of endogenous divalent cations. After mixing with appropriate amount of extra pure $ZnCl_2$ (Fisher Scientific), each buffer was adjusted to pH 7.5 individually due to the acidity of $ZnCl_2$. The assays were performed in sealed Corning 96 well clear bottom half area, nonbinding surface plates and measured by exciting the ThT in samples at 440 nm and reading the emission at 485 nm at a constant temperature of 25°C using BioTek Synergy H1 Hybrid Reader. All kinetic measurements were performed at least in triplicate. The time course data were fitted to an empirical equation to reproduce the change of fluorescent intensity ThT upon binding to the amyloid fibrils (I_{max}-I_0), the apparent rate constant for fibrillization (k), and the lag time ($t_{1/2}$-2/k) to represent the time of nucleation before detectable amyloid formation:

$$I(t) = I_0 + (I_{\max} - I_0) / \{1 + \exp[-k(t - t_{1/2})]\}, \quad (1)$$

where I, I_0 and I_{max} are the reading, initial and maximum fluorescence values, $t_{1/2}$ is the time required to reach half change of intensity.

Results

Modeling zinc-histidine coordination in DMD. Zinc-coordination is known to be covalent-like with both distance and angular dependence. It is not straightforward to directly model the process of zinc binding with proteins in DMD simulations. However, with the availability of a large number of protein structures co-crystallized with zinc ions in the protein data bank (PDB[27]), we first performed statistical analysis of zinc-histidine coordination (Fig. S1) and

assigned constraint potentials between zinc and the imidazole side-chain of histidine to mimic their coordination (Methods). The binding of zinc ions to the NE2 atom of a histidine imidazole ring is more frequent than binding to the ND1 nitrogen (Fig. S1). Since the histidine side chains are rather flexible and the two nitrogen atoms in the imidazole are nearly symmetric, we do not expect inter-peptide interactions to be highly sensitive to which nitrogen zinc ions bind. Hence for simplicity only zinc-NE2 binding was considered. The zinc-imidazole binding is coplanar,[28] which was imposed in DMD by applying additional constraints between zinc ions and all other four imidazole atoms. Following the DMD convention, we used step-functions to model for these constraints (Fig. S2). The corresponding distance parameters were obtained from the inter-atomic distance distributions derived from PDB (Fig. S1). Similarly, the coordination geometry of multiple histidines coordinated to a single zinc ion, e.g. octahedron in the case of hexamer, was maintained by applying distance constraints between NE2 atoms of bound histidines. The ideal angular values of tetrahedral and octahedral coordination spheres were used to model inter-NE2 distance constraints.

Structure and dynamics of zinc-bound hIAPP monomer. A common experimental challenge in structural characterization of hIAPP is its high propensity to form amyloid aggregation. C-terminal residues 22–29 are particularly favorable for amyloid formation and hence hIAPP1–19 is often used as an alternative to full-length hIAPP in structural studies.[29] We performed DMD simulations of zinc-bound and zinc-free hIAPP1–19 peptides for ~50 ns at 300 K. There was no major structural difference between the two systems, as illustrated by their representative structures (Fig. 1A,B) and histograms of the root mean square deviation (RMSD) with respected to the initial NMR structure (PDB ID: 2L86) taken from PDB (Fig. S3). Compared to the zinc-free peptide, the RMSD histogram of zinc-bound hIAPP1–19 was slightly shifted to the right, indicating a small increase in structural deviation upon zinc binding. hIAPP has two positively charged residues (Lys1 and Arg11) near the N-terminal. The slight increase in RMSD upon zinc binding was possibly caused by the electrostatic repulsion between the zinc ion (+2e) and the two N-terminal charged residues. We also calculated the two-dimensional potential mean force (PMF) with respect to RMSD and potential energy, which characterizes the free energy landscapes (Fig. 1C,D). Both PMF plots featured well-defined basins centered near a RMSD value of ~4 Å and energy ~-30 kcal/mol, indicating a well-defined folded structures for both the zinc-bound and zinc-free peptides. Interestingly, despite the similarity between the free energy landscapes of two peptides, the zinc-bound peptide featured a narrower basin, which was consistent with the zinc-induced conformational rigidity observed in NMR.[15]

We also performed additional DMD simulations of full-length hIAPP peptides with and without zinc binding. Similar to the shorter hIAPP1–19, no major difference in secondary structure or RMSD was observed (Fig. S4). Therefore, our DMD simulations suggest that the changes in hIAPP aggregation upon binding zinc ions are not the results of structural changes in hIAPP monomer.

hIAPP oligomers coordinated by zinc. We carried out DMD simulations to model a range of possible hIAPP oligomers — dimer, trimer, tetramer and hexamer — coordinated by a single zinc ion (Methods). Examination of these simulation trajectories indicated differences in structure and dynamics between hexamers and other oligomers. For instance, we noticed that the structures of trimers and tetramers were more flexible, allowing the bound peptides to undergo

structural rearrangements. However, the peptides forming a hexamer were heavily packed against each other near the central His18 residues, restricting their conformational flexibility. Residues 22–29 in hIAPP are believed to be amyloidogenic according to *in vitro* studies.[30] The same region was detected by the amyloid-prediction algorithm, Waltz,[31] and our previous DMD simulations of hIAPP dimerization also suggested that parallel association of hIAPP chains at this region is important for hIAPP aggregation *in silico*.[32] In our DMD simulations of zinc-coordinated hIAPP oligomers, we also observed that these amyloidogenic sequences belonging to different chains make frequent contacts with each another (e.g. representative structures of tetramers and hexamers in Fig. 2A,B, where the amyloidogenic sequences are highlighted in rainbow). Occasionally, parallel β-sheets were formed between the amyloidogenic sequences of different chains, particularly in the cases of trimer and tetramer simulations. Next, we analyzed the aggregation propensity of zinc-coordinated hIAPP oligomers with different MWs.

Aggregation propensity depends on the zinc coordination number. To ensure sufficient sampling of zinc-coordinated oligomer structures, we performed ten independent DMD simulations for each oligomer system where each monomer started from different initial position and orientation (Methods). In all cases, equilibrium DMD simulations were performed at room temperature (300K) and all independent DMD runs for a given oligomer were used for analysis. For comparison, we also performed dimer simulations where each peptide was bound to one zinc ion (hI2-Zn2, corresponding to high zinc/hIAPP ratio) and two peptides with no zinc bound (hI2, corresponding to zero zinc concentration).

A high number of atomic contacts between the amyloidogenic segments from different hIAPP chains translates to a high probability for these peptides to nucleate the formation of amyloid aggregates. Therefore, we first estimated the aggregation propensity of an oligomer by calculating the total number of atomic contacts formed between the amyloidogenic sequences from different chains (Methods). The average number of amyloid contacts per chain, NC_a, was obtained by normalizing with the number of peptides in the oligomer. By averaging over independent simulations, we computed the time-dependence of the NC_a for different zinc-coordinated oligomers (Fig. 3A, Fig. S5). At the beginning of the simulation, the NC_a was proportional to the zinc-coordination number with the hexamer having the highest value. However, as simulations proceeded, an increase of the contact number was observed for dimers, trimers and tetramers, but no apparent increase was observed in the case of hexamers. The difference was due to the inability of hexamer-forming chains to undergo major structural rearrangements.

We averaged over the second half of all trajectories to compute the average NC_a as the increasing order of the zinc:hIAPP ratio (Fig. 3B). The increase in the stoichiometric ratio mimics the increase in relative concentration of zinc ion with respect to hIAPP. As the zinc:hIAPP ratio increases, the average NC_a value first increased, reached a maximum for the tetramer and then decreased. When there was an excess of zinc ions and each hIAPP was bound by one zinc ion, the average amyloidogenic contact number for simulations of two zinc-bound hIAPP monomers (e.g. hI2-Zn2 system in Fig. 3) was close to zero, suggesting a very weak association of two zinc-coordinated monomers. The possible cause for such a weak association probability was the electrostatic repulsion between zinc ions bound to His18, similar to the reduced hIAPP aggregation at low pH where His18 is protonated.[11] For comparison, we also

performed dimer simulations with protonated His18. The charge of a histidine in this case is +1e, smaller than +2e of zinc ion bound to the same histidine. If reduced binding in hI2-Zn2 system was actually caused by electrostatic repulsion between zinc ions, we expected the average contact number of the protonated His18 simulations to be higher than 0.71 (denoted as hI2-Zn2 in Fig. 3B), but lower than 32.5 (denoted as hI2). Indeed, we obtained an intermediate value of 20.9 for the new system (denoted as hI*2 in Fig. 3B).

To directly quantify the inter-molecular β-sheet formation, we monitored the number of inter-chain hydrogen bonds formed by the backbone atoms belonging to the amyloidogenic region. Both the time-dependence (Fig. 3C, Fig. S6) and the time-averaged (Fig. 3D) inter-molecular hydrogen bond numbers had a similar dependency on zinc:hIAPP ratio as the amyloidogenic contact number, NC_a. Notably, the average number of hydrogen bonds per chain was small because the hydrogen bond formation required alignment of peptide chains, which required more time than making contacts. In addition, inter-molecular β-sheets were not always observed in all the independent simulations. In all cases, the number of inter-chain hydrogen bonds averaged over all simulations started from zero and increased after a certain time, analogous to the aggregation lag time observed experimentally.[14,15] Interestingly, the lag time for inter-molecular hydrogen bond formation had a strong dependence on zinc:hIAPP stoichiometry (Table 1). The hexamer had the shortest lag time and the tetramer and trimer had the intermediate lag time, while the lag time for the dimer was the longest. In the case of the dimer, the formed hydrogen bonds were not stable and have large fluctuations, consistent with high conformational flexibility of the zinc-coordinated dimer. Noticeably, the dependence of aggregation amount (Fig. 3B,D) and the lag time (Fig. 3C, Table 1) on zinc concentrations are different. This difference is not surprising since the amount of aggregates is governed by their thermo-stability while the lag time is a kinetics parameter controlled by the free energy barrier.

We also calculated overall secondary structure content of the oligomer system (Fig. S7). Although the secondary structure contents had large fluctuations, the zinc-bound oligomers (dimers, trimers, tetramers, and hexamers) had higher overall helical contents than those of the zinc-bound hIAPP monomer, zinc-free hIAPP at neutral or low pH (with protonated histidines). This observation was consistent with the increase of α-helixes in the oligomer intermediates along the aggregation pathway[33,34] (although experiments were done in the absence of zinc).

The dependence of hIAPP aggregation on zinc concentration measured by the ThT assay. To demonstrate the complex effects of zinc on hIAPP aggregation, we performed an amyloid aggregation kinetics assay with varying concentrations of zinc using 10 μM hIAPP (Methods). ThT is commonly used as a specific marker to recognize β-sheets of amyloid aggregates due to enhanced fluorescence upon binding. The fluorescence intensity quantifies the amount of amyloid aggregates. Fitting the aggregation time-course data (Fig. 4A) with the empirical sigmoidal function (Eq. 1 in Methods), we obtained the maximum fluorescence intensity (Fig. 4B), the elongation rate (Fig. 4C), and the aggregation lag time (Fig. 4D) as the function of zinc concentration. The maximum fluorescence intensity measures the total amount of amyloid aggregates. At low zinc concentrations (<50 μM; Fig. 4B), addition of zinc resulted in increased aggregation. At higher zinc concentrations, zinc starts to inhibit aggregation. A plateau in zinc concentration ranging from 7.5 to 15 μM was observed. At the plateau, the aggregation was 1.5-fold greater than that in the absence of zinc (Fig. 4B). The maximal reduction of aggregation was

observed at 750 μM to 15 mM zinc, which was 3.2-fold less than that at plateau. The amyloid fibrils formation can be viewed as a two-step process in which the lag phase entails nucleation followed by an elongation phase. Despite a weaker dependence on zinc concentration compared to the maximum fluorescence intensity (i.e. the amount of aggregates; Fig. 4B), the elongation rate showed a similar initial increase followed by subsequent reduction over the range of zinc concentrations (Fig. 4C). Interestingly, despite the increased total aggregation amount and enhanced elongation rate at low zinc concentrations, the initial lag time till the appearance of aggregates was delayed (Fig. 4D).

Discussion

This combined computational and experimental study intended to uncover the controversial role of zinc on hIAPP aggregation and T2D development. Our computational results are consistent with experimentally observed dependence of hIAPP aggregation on zinc concentrations. At very low zinc:hIAPP ratios, zinc-coordinated hIAPP oligomers are dominated by high MW (HMW) species, such as hexamers. The increase of relative zinc concentration shifts the population toward lower MW oligomers. Once there are excessive zinc ions, the dominant species become the zinc-bound hIAPP monomers. Our computational study of hIAPP oligomers with different MWs suggests an initial increase of aggregation amount followed by a decrease (Fig. 3A,B), which is consistent with the experimentally observed dependence of ThT fluorescence intensity on zinc concentration (Fig. 4B). At high zinc:hIAPP ratios, the concentration of the aggregating species, i.e. zinc-bound hIAPP monomers, is determined by the peptide concentration. At low zinc:hIAPP ratios, the concentration of the aggregating zinc-bound oligomers is governed by the zinc concentration. Therefore, according to our model, the aggregation becomes more peptide-concentration dependent at high zinc concentrations. Interestingly, a previous experimental study with different concentrations of hIAPP demonstrated this differential peptide-concentration dependence (see Fig. 2 in Ref.[14]), in agreement with our model.

The lag times measured in simulations (Fig. 3C and Table 1) and in experiments (Fig. 4D) correspond to two different quantities. *In silico* the lag time of hydrogen bond formation is measured from the point of oligomer formation whereas *in vitro* the total lag time of aggregation, including the time for oligomer formation, is measured. It is still intriguing that these two quantities follow a similar overall trend with respect to the zinc:hIAPP ratio. It should also be noted that at very high zinc concentration a weak recovery in the total aggregation amount with increasing zinc concentration was reported previously,[14,15] but such an increase was within error bar in our experimental study (Fig. 4B). This recovery of aggregation is possibly due to increased screening effect with added chloride ions, which results in reduced electrostatic repulsion between the hIAPP-bound zinc ions. Therefore, without introducing a second zinc-binding site that promotes aggregation,[15] our model with one zinc-binding site can already explain the complex dependence of hIAPP aggregation on a wide range of zinc concentrations. Similar to its effect on hIAPP aggregation, zinc and other divalent metal ions (e.g. copper and magnesium) also display complex effects on amyloid formation by other proteins such as amyloid-β and α-synuclein.[35–37] For instance, low concentration of zinc was found to increase the amount of amyloid-β fibril and reduce the oligomer content, but did not significantly affect the monomer concentration. Since both amyloid-β and α-synuclein have more than one zinc-binding

residue, it is likely that zinc binding may affect the stabilities of monomers, oligomers and fibrils differently. Further studies are required for a complete understanding of the impacts of divalent ions on the aggregation of these amyloidogenic proteins at the molecular level.

Our results can help explain previous experimental observations with contradicting effect of zinc on IAPP aggregation. The major differences between the Steiner[9] and Ramamoorthy[14] studies were the concentrations of IAPP and the relative stoichiometry between zinc and IAPP. The affinity between zinc and IAPP is of the order of ~μM.[15] With low concentrations of IAPP (e.g. 5–10 μM in Ref.[14]), sufficient binding with the peptide requires a relatively high concentration of zinc and thus a relatively high zinc:hIAPP stoichiometry. For example, in the case of 5 μM hIAPP, the relatively high zinc:hIAPP stoichiometry probably allowed the formation of zinc-bound hIAPP monomers only, which inhibits IAPP aggregation. With 10 μM, it was possible to observe the initial promotion of aggregation due to the formation of higher-order zinc-coordinated hIAPP oligomers. In the aggregation study with 250 μM hIAPP,[9] the authors were able to observe the concentration-dependent protein aggregation for a wide range of zinc concentrations.

In addition to hIAPP and zinc inside β-cell granules, there are high concentrations of other molecules, such as insulin and C-peptides.[38] C-peptide is the co-product of insulin synthesis, which connects A- and B-chains of insulin in the precursor protein, proinsulin. C-peptide and insulin are secreted at equal molar concentrations. We hypothesize that inter-molecular interactions among these granular molecules are important for the native inhibition of hIAPP aggregation *in vivo*. For example, zinc is highly active and can bind all three granular proteins, hIAPP,[14,15] insulin[39,40] and C-peptide.[41,42] Zinc is known to regulate the oligomer equilibrium of insulin between zinc-free monomers and dimers, and zinc-coordinated hexamers. The insulin hexamer is found to be insoluble and form crystals inside the granule. In a previous computational study,[32] we showed that soluble insulin monomers and dimers could form inter-molecular complexes with hIAPP and inhibit hIAPP self-association and aggregation by competing for the same hIAPP sequence (e.g., the amyloidogenic sequence of residues 22–29). Therefore, zinc deficiency shifts the equilibrium of insulin hexamers to monomers and dimmers and inhibits hIAPP aggregation, which explains the recently reported protection from T2D for the loss-of-function mutations of ZnT8. In this work, our combined computational and experimental study suggests that direct binding of zinc ions with hIAPP may contribute to the zinc-dependent inhibition of hIAPP aggregation at the high zinc concentrations. Therefore, in the case of mutations that only perturb the activity of ZnT8 where the base-line of zinc concentration is high (e.g. W325R in ZnT8[12]), an anti-correlation between zinc concentration and hIAPP aggregation propensity is expected, which helps explain the observation of increased T2D risk with activity-reducing mutations of ZnT8.

In summary, using atomistic DMD simulations combined with experimental validation, our study uncovers the molecular mechanism for the complex role of direct zinc binding on IAPP aggregation and T2D development (Fig 5). At low zinc concentrations with low zinc:hIAPP stoichiometry ratios, zinc ion coordinates the formation of HMW oligomers of hIAPP, which are aggregation-prone due to high local hIAPP concentration. As the stoichiometry increases, each zinc ion can only bind to individual hIAPP. The zinc-bound hIAPP monomer has a lower propensity to self-associate and aggregate due to strong electrostatic

repulsion between the zinc ions bound to His18 (+2e). The mechanism is similar to the reduced hIAPP aggregation at low pH, where the same histidine residue is protonated (+e). At very high zinc concentrations, the added salt increases the electrostatic screening effect, which reduces the repletion between the zinc-coordinated hIAPP monomers and promotes aggregation. Our results help explain the "*seemingly contradicting*" correlations between ZnT8 activity and T2D risk at the population level. Our combined computational and experimental study suggests that it is necessary to fully understand the complex role of zinc ions on hIAPP aggregation *in vitro* and *in vivo* in order to design effective therapeutics, e.g. targeting ZnT8 with agonists or antagonists, and demonstrates that computational studies may be of great help in such a process.

Funding. The work is supported in part by NSF CBET-1232724, NIH R15ES022766-01A1, and the startup funds from Clemson University.

Acknowledgements
All simulations were performed on the Palmetto high performance cluster, which is managed and maintained by Clemson University CCIT.

Supporting Information
Zn-imidazole bond parameters, histogram of Zn-Histidine bond lengths (PDB database), schematic of potential modeling Zn-Histidine bond, RMSD distribution of hIAPP1-19, hIAPP secondary structure contents, amyloidogenic contact and hydrogen bond numbers and secondary structure contents of Zn-coordinated hIAPP oligomers.

References

(1) Höppener, J. W. M., Ahrén, B., and Lips, C. J. M. (2000) Islet Amyloid and Type 2 Diabetes Mellitus. *N. Engl. J. Med. 343*, 411–419.
(2) Höppener, J. W. M., and Lips, C. J. M. (2006) Role of islet amyloid in type 2 diabetes mellitus. *Int. J. Biochem. Cell Biol. 38*, 726–736.
(3) Schmitz, O., Brock, B., and Rungby, J. (2004) Amylin Agonists: A Novel Approach in the Treatment of. *Diabetes 53*, S233–S238.
(4) Kahn, S. E., Andrikopoulos, S., and Verchere, C. B. (1999) Islet amyloid: a long-recognized but underappreciated pathological feature of type 2 diabetes. *Diabetes 48*, 241–253.
(5) Zraika, S., Hull, R. L., Verchere, C. B., Clark, A., Potter, K. J., Fraser, P. E., Raleigh, D. P., and Kahn, S. E. (2010) Toxic oligomers and islet beta cell death: guilty by association or convicted by circumstantial evidence? *Diabetologia 53*, 1046–1056.
(6) Ritzel, R. A., Meier, J. J., Lin, C.-Y., Veldhuis, J. D., and Butler, P. C. (2007) Human Islet Amyloid Polypeptide Oligomers Disrupt Cell Coupling, Induce Apoptosis, and Impair Insulin Secretion in Isolated Human Islets. *Diabetes 56*, 65–71.
(7) Padrick, S. B., and Miranker, A. D. (2002) Islet Amyloid: Phase Partitioning and Secondary Nucleation Are Central to the Mechanism of Fibrillogenesis†. *Biochemistry (Mosc.) 41*, 4694–4703.

(8) Nishi, M., Sanke, T., Nagamatsu, S., Bell, G. I., and Steiner, D. F. (1990) Islet amyloid polypeptide. A new beta cell secretory product related to islet amyloid deposits. *J. Biol. Chem. 265*, 4173–4176.
(9) Westermark, P., Li, Z.-C., Westermark, G. T., Leckström, A., and Steiner, D. F. (1996) Effects of beta cell granule components on human islet amyloid polypeptide fibril formation. *FEBS Lett. 379*, 203–206.
(10) Larson, J. L., and Miranker, A. D. (2004) The Mechanism of Insulin Action on Islet Amyloid Polypeptide Fiber Formation. *J. Mol. Biol. 335*, 221–231.
(11) Jha, S., Snell, J. M., Sheftic, S. R., Patil, S. M., Daniels, S. B., Kolling, F. W., and Alexandrescu, A. T. (2014) pH Dependence of Amylin Fibrillization. *Biochemistry (Mosc.) 53*, 300–310.
(12) Nicolson, T. J., Bellomo, E. A., Wijesekara, N., Loder, M. K., Baldwin, J. M., Gyulkhandanyan, A. V., Koshkin, V., Tarasov, A. I., Carzaniga, R., Kronenberger, K., Taneja, T. K., Xavier, G. da S., Libert, S., Froguel, P., Scharfmann, R., Stetsyuk, V., Ravassard, P., Parker, H., Gribble, F. M., Reimann, F., Sladek, R., Hughes, S. J., Johnson, P. R. V., Masseboeuf, M., Burcelin, R., Baldwin, S. A., Liu, M., Lara-Lemus, R., Arvan, P., Schuit, F. C., Wheeler, M. B., Chimienti, F., and Rutter, G. A. (2009) Insulin Storage and Glucose Homeostasis in Mice Null for the Granule Zinc Transporter ZnT8 and Studies of the Type 2 Diabetes–Associated Variants. *Diabetes 58*, 2070–2083.
(13) Foster, M. C., Leapman, R. D., Li, M. X., and Atwater, I. (1993) Elemental composition of secretory granules in pancreatic islets of Langerhans. *Biophys. J. 64*, 525–532.
(14) Brender, J. R., Hartman, K., Nanga, R. P. R., Popovych, N., de la Salud Bea, R., Vivekanandan, S., Marsh, E. N. G., and Ramamoorthy, A. (2010) Role of Zinc in Human Islet Amyloid Polypeptide Aggregation. *J. Am. Chem. Soc. 132*, 8973–8983.
(15) Salamekh, S., Brender, J. R., Hyung, S.-J., Nanga, R. P. R., Vivekanandan, S., Ruotolo, B. T., and Ramamoorthy, A. (2011) A Two-Site Mechanism for the Inhibition of IAPP Amyloidogenesis by Zinc. *J. Mol. Biol. 410*, 294–306.
(16) Sladek, R., Rocheleau, G., Rung, J., Dina, C., Shen, L., Serre, D., Boutin, P., Vincent, D., Belisle, A., Hadjadj, S., Balkau, B., Heude, B., Charpentier, G., Hudson, T. J., Montpetit, A., Pshezhetsky, A. V., Prentki, M., Posner, B. I., Balding, D. J., Meyre, D., Polychronakos, C., and Froguel, P. (2007) A genome-wide association study identifies novel risk loci for type 2 diabetes. *Nature 445*, 881–885.
(17) Flannick, J., Thorleifsson, G., Beer, N. L., Jacobs, S. B. R., Grarup, N., Burtt, N. P., Mahajan, A., Fuchsberger, C., Atzmon, G., Benediktsson, R., Blangero, J., Bowden, D. W., Brandslund, I., Brosnan, J., Burslem, F., Chambers, J., Cho, Y. S., Christensen, C., Douglas, D. A., Duggirala, R., Dymek, Z., Farjoun, Y., Fennell, T., Fontanillas, P., Forsén, T., Gabriel, S., Glaser, B., Gudbjartsson, D. F., Hanis, C., Hansen, T., Hreidarsson, A. B., Hveem, K., Ingelsson, E., Isomaa, B., Johansson, S., Jørgensen, T., Jørgensen, M. E., Kathiresan, S., Kong, A., Kooner, J., Kravic, J., Laakso, M., Lee, J.-Y., Lind, L., Lindgren, C. M., Linneberg, A., Masson, G., Meitinger, T., Mohlke, K. L., Molven, A., Morris, A. P., Potluri, S., Rauramaa, R., Ribel-Madsen, R., Richard, A.-M., Rolph, T., Salomaa, V., Segrè, A. V., Skärstrand, H., Steinthorsdottir, V., Stringham, H. M., Sulem, P., Tai, E. S., Teo, Y. Y., Teslovich, T., Thorsteinsdottir, U., Trimmer, J. K., Tuomi, T., Tuomilehto, J., Vaziri-Sani, F., Voight, B. F., Wilson, J. G., Boehnke, M., McCarthy, M. I., Njølstad, P. R., Pedersen, O., Go-T2D Consortium, T2d-Genes Consortium, Groop, L., Cox, D. R., Stefansson, K., and Altshuler, D.

(2014) Loss-of-function mutations in SLC30A8 protect against type 2 diabetes. *Nat. Genet. 46*, 357–363.
(18) Shirvanyants, D., Ding, F., Tsao, D., Ramachandran, S., and Dokholyan, N. V. (2012) Discrete Molecular Dynamics: An Efficient And Versatile Simulation Method For Fine Protein Characterization. *J. Phys. Chem. B 116*, 8375–8382.
(19) Ding, F., Tsao, D., Nie, H., and Dokholyan, N. V. (2008) Ab Initio Folding of Proteins with All-Atom Discrete Molecular Dynamics. *Structure 16*, 1010–1018.
(20) Dagliyan, O., Proctor, E. A., D'Auria, K. M., Ding, F., and Dokholyan, N. V. (2011) Structural and Dynamic Determinants of Protein-Peptide Recognition. *Structure 19*, 1837–1845.
(21) Lazaridis, T., and Karplus, M. (1999) Effective energy function for proteins in solution. *Proteins Struct. Funct. Bioinforma. 35*, 133–152.
(22) Andersen, H. C. (1980) Molecular dynamics simulations at constant pressure and/or temperature. *J. Chem. Phys. 72*, 2384–2393.
(23) Laitaoja, M., Valjakka, J., and Jänis, J. (2013) Zinc Coordination Spheres in Protein Structures. *Inorg. Chem. 52*, 10983–10991.
(24) Maret, W., and Li, Y. (2009) Coordination dynamics of zinc in proteins. *Chem. Rev. 109*, 4682–4707.
(25) Alberts, I. L., Nadassy, K., and Wodak, S. J. (1998) Analysis of zinc binding sites in protein crystal structures. *Protein Sci. Publ. Protein Soc. 7*, 1700–1716.
(26) Nanga, R. P. R., Brender, J. R., Vivekanandan, S., and Ramamoorthy, A. (2011) Structure and membrane orientation of IAPP in its natively amidated form at physiological pH in a membrane environment. *Biochim. Biophys. Acta BBA - Biomembr. 1808*, 2337–2342.
(27) Berman, H. M., Westbrook, J., Feng, Z., Gilliland, G., Bhat, T. N., Weissig, H., Shindyalov, I. N., and Bourne, P. E. (2000) The Protein Data Bank. *Nucleic Acids Res. 28*, 235–242.
(28) Mera-Adasme, R., Sadeghian, K., Sundholm, D., and Ochsenfeld, C. (2014) Effect of Including Torsional Parameters for Histidine–Metal Interactions in Classical Force Fields for Metalloproteins. *J. Phys. Chem. B*.
(29) Brender, J. R., Lee, E. L., Cavitt, M. A., Gafni, A., Steel, D. G., and Ramamoorthy, A. (2008) Amyloid Fiber Formation and Membrane Disruption are Separate Processes Localized in Two Distinct Regions of IAPP, the Type-2-Diabetes-Related Peptide. *J. Am. Chem. Soc. 130*, 6424–6429.
(30) Tenidis, K., Waldner, M., Bernhagen, J., Fischle, W., Bergmann, M., Weber, M., Merkle, M.-L., Voelter, W., Brunner, H., and Kapurniotu, A. (2000) Identification of a penta- and hexapeptide of islet amyloid polypeptide (IAPP) with amyloidogenic and cytotoxic properties. *J. Mol. Biol. 295*, 1055–1071.
(31) Maurer-Stroh, S., Debulpaep, M., Kuemmerer, N., Paz, M. L. de la, Martins, I. C., Reumers, J., Morris, K. L., Copland, A., Serpell, L., Serrano, L., Schymkowitz, J. W. H., and Rousseau, F. (2010) Exploring the sequence determinants of amyloid structure using position-specific scoring matrices. *Nat. Methods 7*, 237–242.
(32) Nedumpully-Govindan, P., and Ding, F. (2015) Inhibition of IAPP aggregation by insulin depends on the insulin oligomeric state regulated by zinc ion concentration. *Sci. Rep. 5,* 8240.
(33) Williamson, J. A., and Miranker, A. D. (2007) Direct detection of transient α-helical states in islet amyloid polypeptide. *Protein Sci. 16*, 110–117.
(34) Abedini, A., and Raleigh, D. P. (2009) A role for helical intermediates in amyloid formation by natively unfolded polypeptides? *Phys. Biol. 6*, 015005.

(35) Cuajungco, M. P., and Fagét, K. Y. (2003) Zinc takes the center stage: its paradoxical role in Alzheimer's disease. *Brain Res. Rev. 41*, 44–56.
(36) Garai, K., Sengupta, P., Sahoo, B., and Maiti, S. (2006) Selective destabilization of soluble amyloid β oligomers by divalent metal ions. *Biochem. Biophys. Res. Commun. 345*, 210–215.
(37) Wang, X., Moualla, D., Wright, J. A., and Brown, D. R. (2010) Copper binding regulates intracellular alpha-synuclein localisation, aggregation and toxicity. *J. Neurochem. 113*, 704–714.
(38) DeToma, A. S., Salamekh, S., Ramamoorthy, A., and Lim, M. H. (2012) Misfolded proteins in Alzheimer's disease and type II diabetes. *Chem. Soc. Rev. 41*, 608–621.
(39) Chang, X., Jørgensen, A. M. M., Bardrum, P., and Led, J. J. (1997) Solution Structures of the R6 Human Insulin Hexamer†,‡. *Biochemistry (Mosc.) 36*, 9409–9422.
(40) Dunn, M. F. (2005) Zinc–Ligand Interactions Modulate Assembly and Stability of the Insulin Hexamer – A Review. *Biometals 18*, 295–303.
(41) Keltner, Z., Meyer, J. A., Johnson, E. M., Palumbo, A. M., Spence, D. M., and Reid, G. E. (2010) Mass spectrometric characterization and activity of zinc-activated proinsulin C-peptide and C-peptide mutants. *Analyst 135*, 278–288.
(42) Meyer, J. A., Subasinghe, W., Sima, A. A. F., Keltner, Z., Reid, G. E., Daleke, D., and Spence, D. M. (2009) Zinc-activated C-peptide resistance to the type 2 diabetic erythrocyte is associated with hyperglycemia-induced phosphatidylserine externalization and reversed by metformin. *Mol. Biosyst. 5*, 1157.

Tables

Table 1. Kinetic parameters for the inter-peptide hydrogen bond formation in DMD simulations. The average number of inter-peptide hydrogen bonds per chain as a function of time (Fig. S6) is fitted using the sigmoidal function (Eq. 1). The fitted values for the parameters – I_0, I_{max}, k, and $t_{1/2}$ – for different hIAPP-zinc oligomer systems are listed below. The lag time, t_{lag}, is calculated as $t_{1/2}$-2/k.

	I_0	I_{max}	k (ns^{-1})	$t_{1/2}$ (ns)	t_{lag}
hI2-Zn	0.017	0.169	2.33	14.98	14.12
hI3-Zn	0.006	0.983	0.41	15.27	10.40
hI4-Zn	0.043	1.108	0.45	14.15	9.68
hI6-Zn	0.160	0.832	1.94	7.18	6.15

Figure Legends

Figure 1. **Zinc-coordinated hIAPP monomer.** Representative structures of hIAPP1–19 monomer (A) without and (B) with zinc-binding in cartoon representation. The highlighted residue corresponds to His18, which binds to a zinc ion shown in sphere. Based on DMD simulations at room temperature, 2D PMFs with respect to potential energy and RMSD with respect to the initial NMR structure (PDB ID: 2L86) are computed for the (C) zinc-free and (D) zinc-bound peptides.

Figure 2. **Zinc-coordinated hIAPP oligomer**. Representative structures of (A) tetramer and (B) hexamer in carton representation are taken from DMD simulations at the room temperature. The zinc ion is shown as blue sphere and the His18 residues as pink sticks. The amyloidogenic sequences (residues 22-29) from each monomer are highlighted in rainbow colors.

Figure 3. **Aggregation propensity of zinc-coordinated hIAPP oligomers derived from DMD simulations.** (A) The number of inter-chain amyloidogenic contact per chain (NC_a) as a function of simulation time, averaged over 10 independent DMD. The label index indicates the molecular composition of the corresponding simulations. For example, hI2-Zn corresponds to two zinc-coordinated hIAPP dimer. (B) The time-averaged amyloidogenic contact per chain is computed for oligomers of different MWs. For comparison, the results for dimer simulations of zinc-free hIAPP monomers (denoted as hI2), zinc-coordinated hIAPP monomers (hI2-Zn2), and hIAPP monomers with protonated His18 (hI*2) are also included. The schematic diagrams illustrate the composition of molecules in each case. (C) The number of backbone hydrogen bonds (H-bond) formed by the amyloidogenic residues per chain as the function of simulation time, averaged over independent DMD simulations. The dashed lines denote the sigmoidal fit using Eq. 1. (D) The average number of H-bonds per chain is calculated for different molecular systems. For illustration purpose, a running average with a sliding window of 0.5 ns was used to reduce noise in panels A and C. The corresponding raw data without running average are shown in Figs. S6 and S7.

Figure 4. The dependence of hIAPP aggregation on zinc concentration *in vitro* using the ThT assay. (A) The normalized ThT fluorescence intensity as the function of time. Experimental measurements at different zinc concentrations and the corresponding sigmoidal fitting are shown in different colors. Only a subset of measurements is presented here for illustration purposes. Fitted with the empirical sigmoidal curve (Eq. 1), aggregation parameters including (B) maximum intensity, (C) elongation rate, and (D) the lag time are calculated as functions of zinc concentration in the linear-log plot. The shaded regions correspond to control experiments without zinc, which otherwise cannot fit to the log scale. Dash line indicated the average value of each parameter in the absence of zinc. Error bars represented the standard deviation of four replicas of measurements at each zinc concentration.

Figure 5. The mechanistic scheme for the complex role of zinc on hIAPP aggregation. At low Zn:hIAPP ratio with low $ZnCl_2$ concentration, a zinc ion shown as the dark green sphere binds multiple hIAPP molecules and increase the probability for the amyloidogenic sequences to form β-sheet rich aggregates. As the zinc concentration increases and there are excessive zinc ions in solution, each zinc tends to only individual hIAPP and electrostatic repulsion between the coordinated zinc ions inhibits aggregation. At very high concentrations, aggregation is recovered

due to reduced electrostatic repulsion with increased screening effect at high salt concentration.

Figures

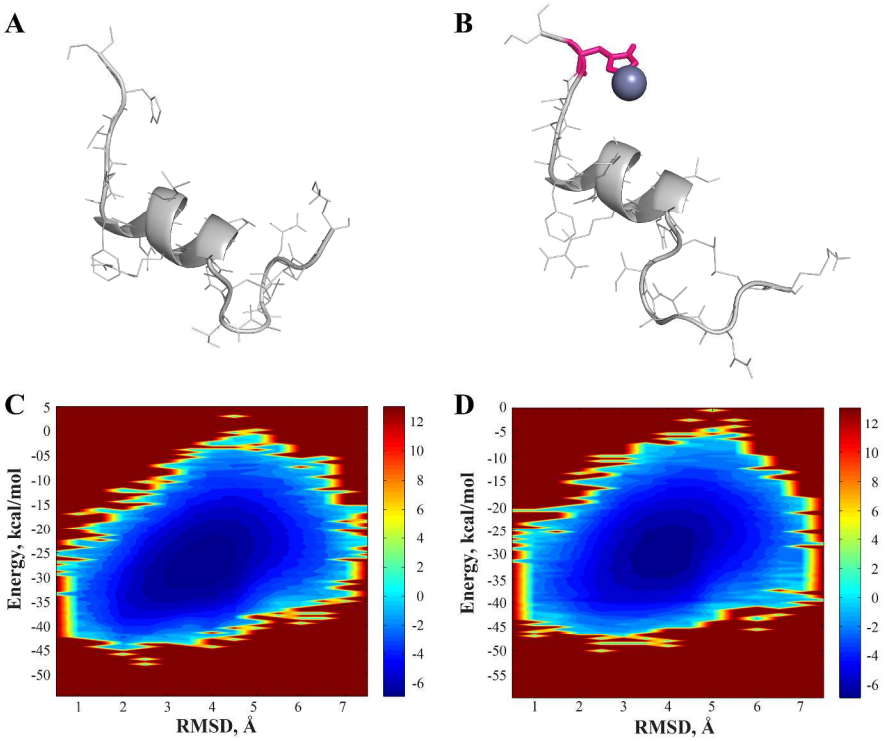

Figure 1

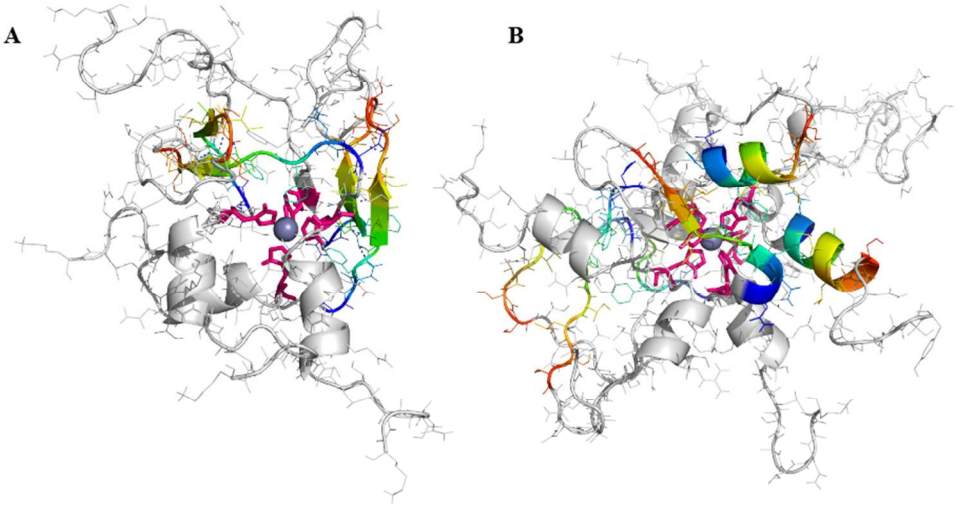

Figure 2

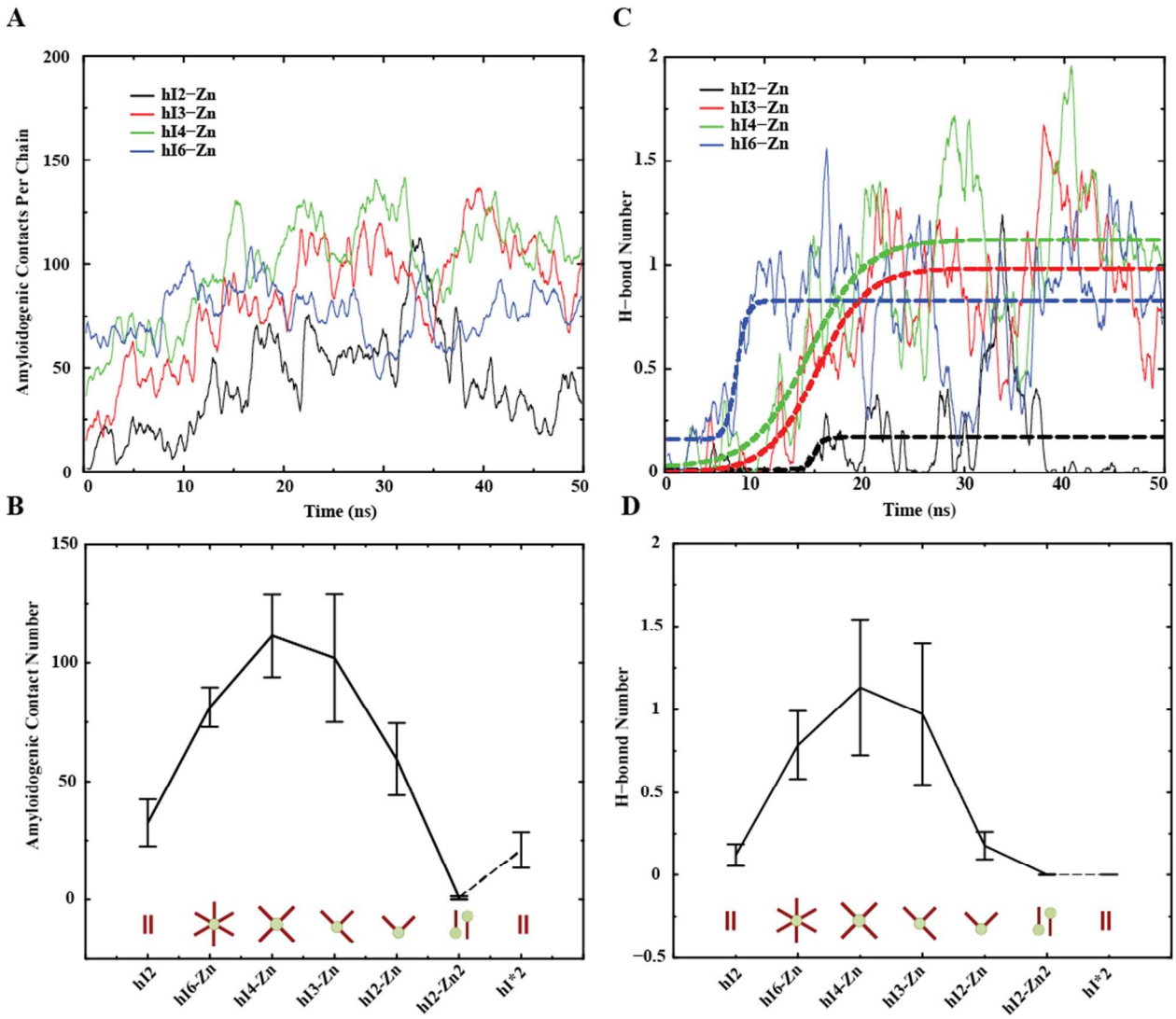
A
C
B
D
hI2−Zn
hI3−Zn
hI4−Zn
hI6−Zn
Amyloidogenic Contacts Per Chain
Time (ns)
H−bond Number
Amyloidogenic Contact Number
H−bonnd Number
hI2
hI6-Zn
hI4-Zn
hI3-Zn
hI2-Zn
hI2-Zn2
hI*2

Figure 3

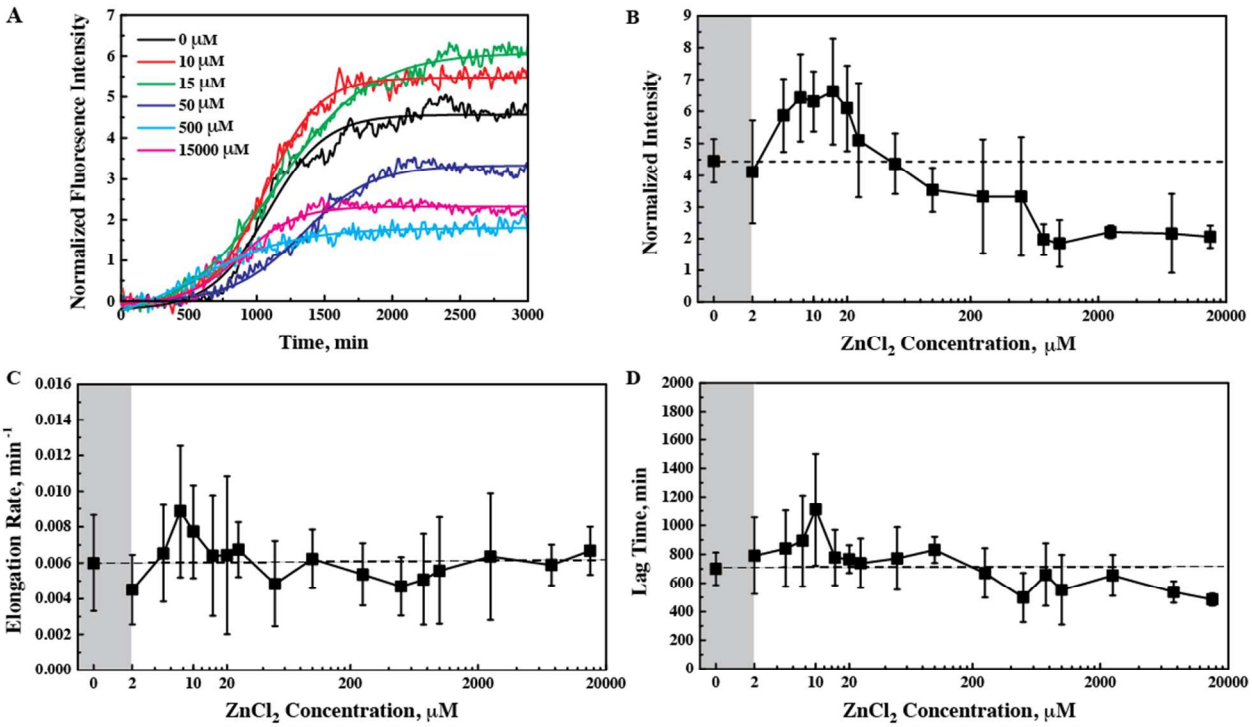
A
Normalized Fluorescence Intensity
Time, min
0 μM
10 μM
15 μM
50 μM
500 μM
15000 μM
B
Normalized Intensity
ZnCl2 Concentration, μM
C
Elongation Rate, min-1
ZnCl2 Concentration, μM
D
Lag Time, min
ZnCl2 Concentration, μM

Figure 4

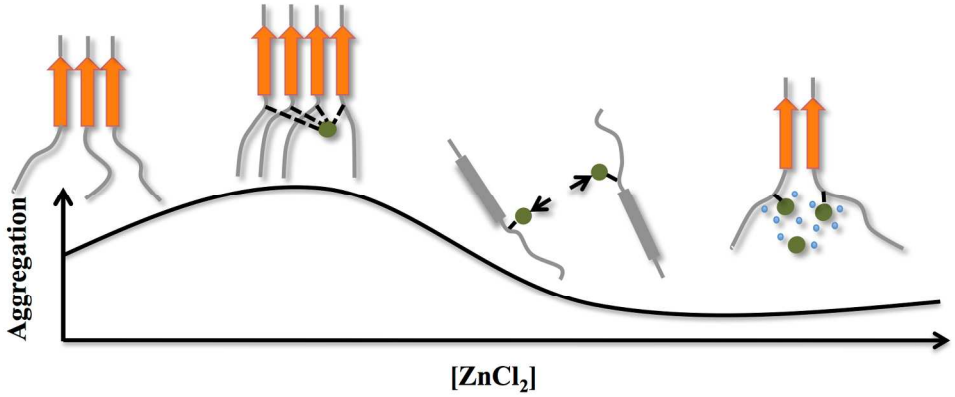

Figure 5

Graphic for the Table of Contents

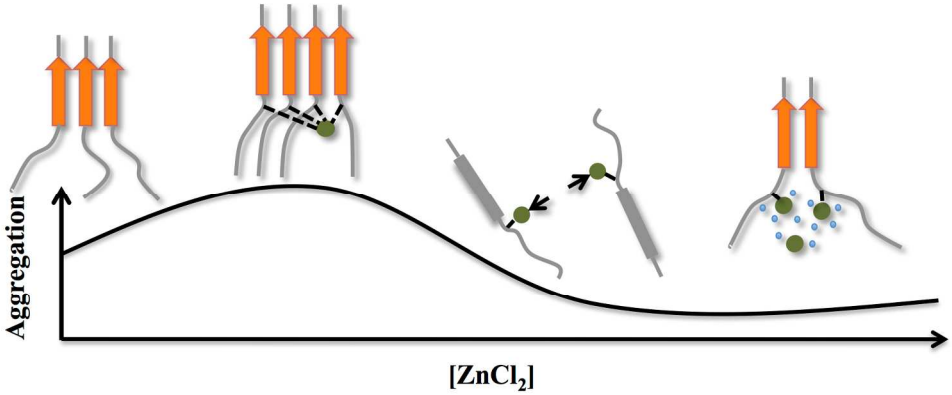

Promotion or Inhibition of IAPP Aggregation by Zinc Coordination Depends on Its Relative Concentration

Praveen Nedumpully-Govindan[a], Ye Yang[b], Rachel Andorfer[a], Weiguo Cao[b], and Feng Ding[a,1]

[a]Department of Physics and Astronomy, Clemson University, Clemson, SC 29634
[b]Department of Biochemistry and Genetics, Clemson University, Clemson, SC 29634
[1]Corresponding Author: fding@clemson.edu; Tel: 864-656-0459

Supplementary Tables

Table S1. Zinc-Imidazole bond parameters. The interaction parameters were obtained from statistical analysis of zinc-histidine binding in PDB (Fig. S1). An infinite square-well potential bound by dmin and dmax was used constrain bond lengths (Fig. S2). The values of d_{min} and d_{max} were obtained by fitting the highest peak in the histograms of Fig. S2. In the case of multiple hIAPPs binding to a zinc ion, His-zinc-His angle was also maintained by applying additional constraints between NE2 atoms of His residues. The NE2-NE2 ideal lengths were calculated using the NE2-zinc coordination bond lengths and ideal tetrahedral (109.5°, for dimer, trimer and tetramer hIAPP coordinated by zinc) or octahedral angles (90° and 180°, for hexamer hIAPP coordinated by zinc).

Bond	**d_{min}(Å)**	**d_{max} (Å)**
Zn-NE2	2.04	2.20
Zn-ND1	4.08	4.30
Zn-CD2	2.98	3.16
Zn-CE1	2.96	3.16
Zn-CG	4.12	4.28
NE2-NE2 (tetrahedral, 109.5°)	3.33	3.59
NE2-NE2 (octahedral, 90°)	2.89	3.11
NE2-NE2 (octahedral, 180°)	4.08	4.40

Supplementary Figures

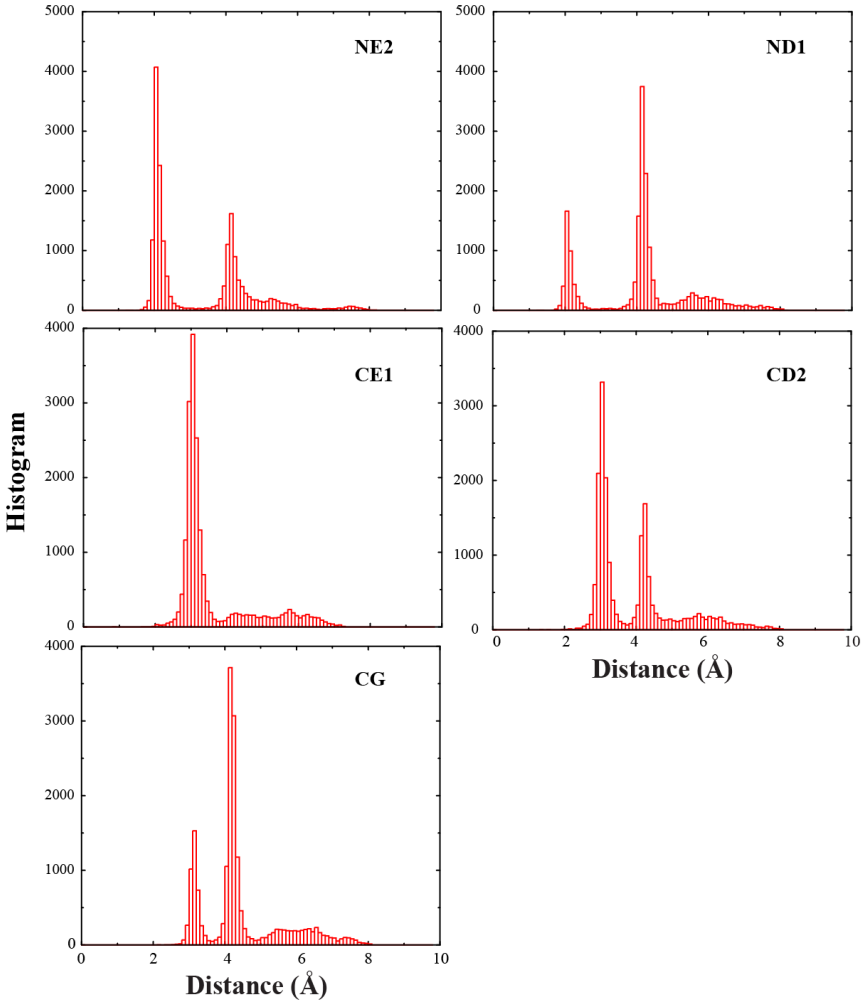

Figure S1. Zn-His coordination bond lengths. The bond length distribution for the coordination bond between zinc and histidine imidazole ring atoms. The distribution is obtained using 9547 zinc containing structures in the PDB. Zinc can bind to either NE2 or ND1 atom of imidazole, giving raise to two peaks. The zinc-NE2 binding seems to be more common as seen in the peak values and hence only zinc-NE2 binding, with a coordination bond length of ~2.1 Å, was considered in simulations. Because of the rigid nature of coordination bond, the distance with the other imidazole atoms also has specific values. We chose the distance corresponding to the highest peak in our model (Table S1).

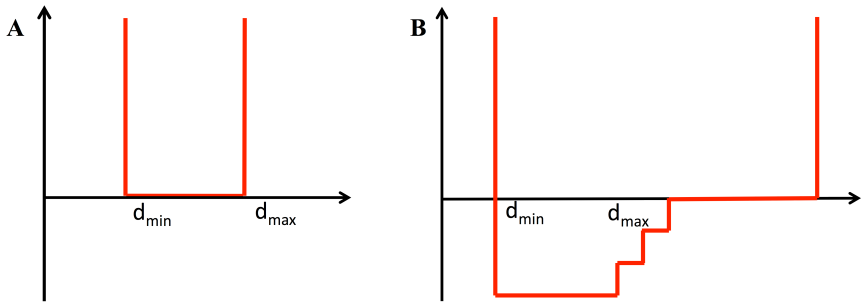

Figure S2. Modeling Zn-His coordination bond. (A) Schematic of the square-well potential used to model coordination bonds between zinc ion and imidazole atoms. dmin and dmax values obtained from Fig. S1 are listed in Table 1. (B) At the beginning of each simulation, a 10,000 steps long simulation is performed with a weak attractive potential between zinc and NE2 atoms of His18. This step is necessary to bring the histidines close to zinc.

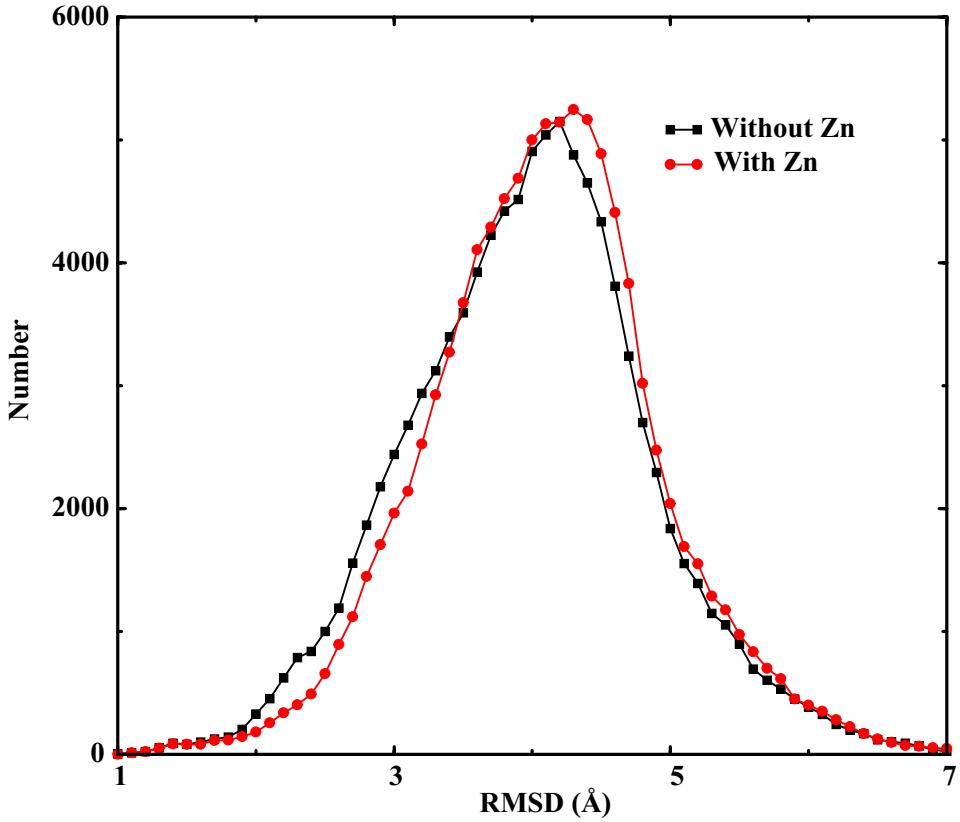

Figure S3. The effect of zinc binding on hIAPP1–19. The distribution of RMSD values of hIAPP1–19 with and without zinc binding. When zinc ion binds the His18 residues, a small shift of RMSD curve to the right is observed, likely due to electrostatic repulsion between zinc ions and two positively charged residues (Lys1 and Arg11).

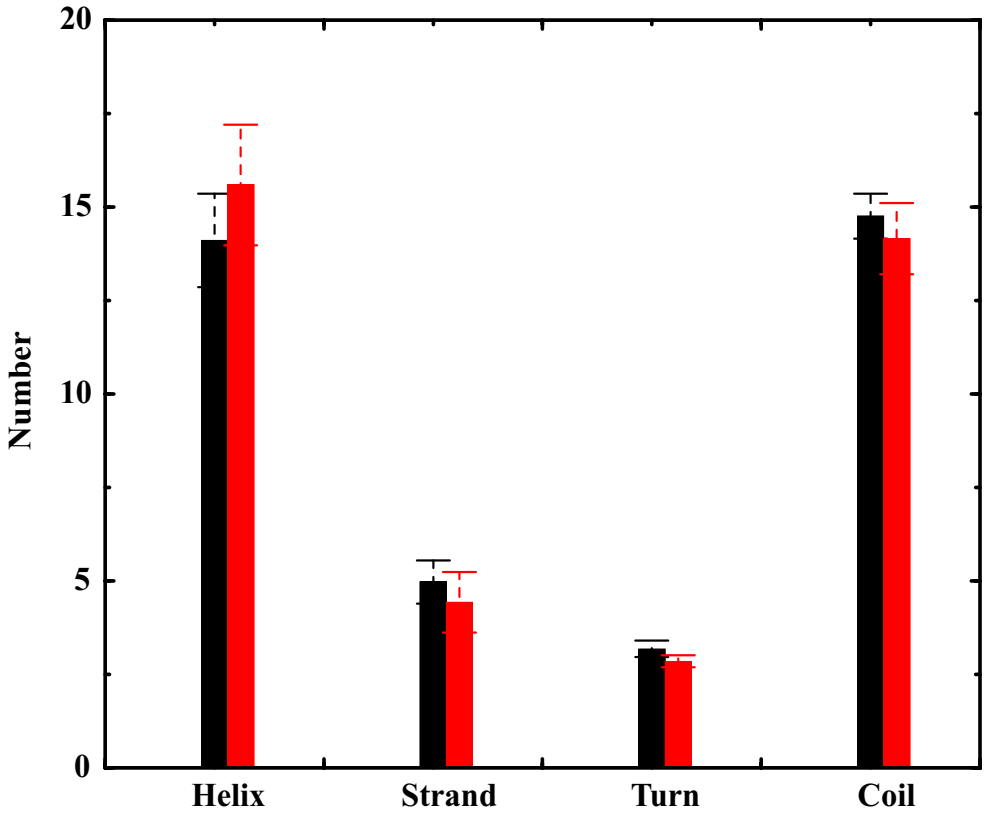

Figure S4. The effect of zinc binding on hIAPP1–37. The secondary structure contents of full-length hIAPP monomers with (red) and without (black) a bound zinc ion. In the zinc-bound case, a small increase of helical content and a decrease of coil content are observed. The error bars represent standard error of measurements from ten independent simulations.

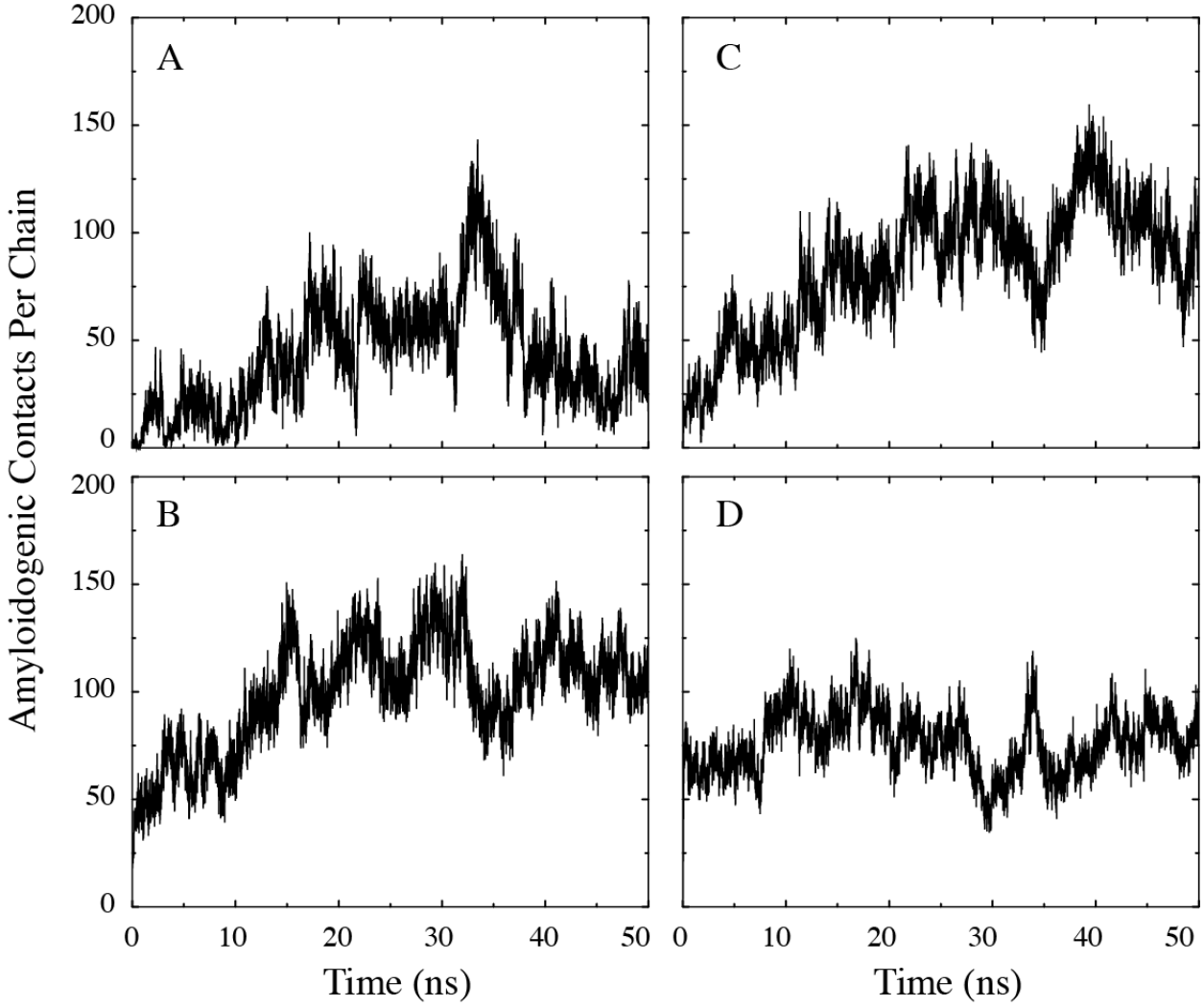

Figure S5. Time dependent amyloid contact number. The amyloid contact number per chain for different systems as a function of time for simulations of (A) hI2-Zn, (B) hI3-Zn, (C) hI4-Zn, and (D) hI6-Zn. The instantaneous contact number is averaged over 10 independent simulations.

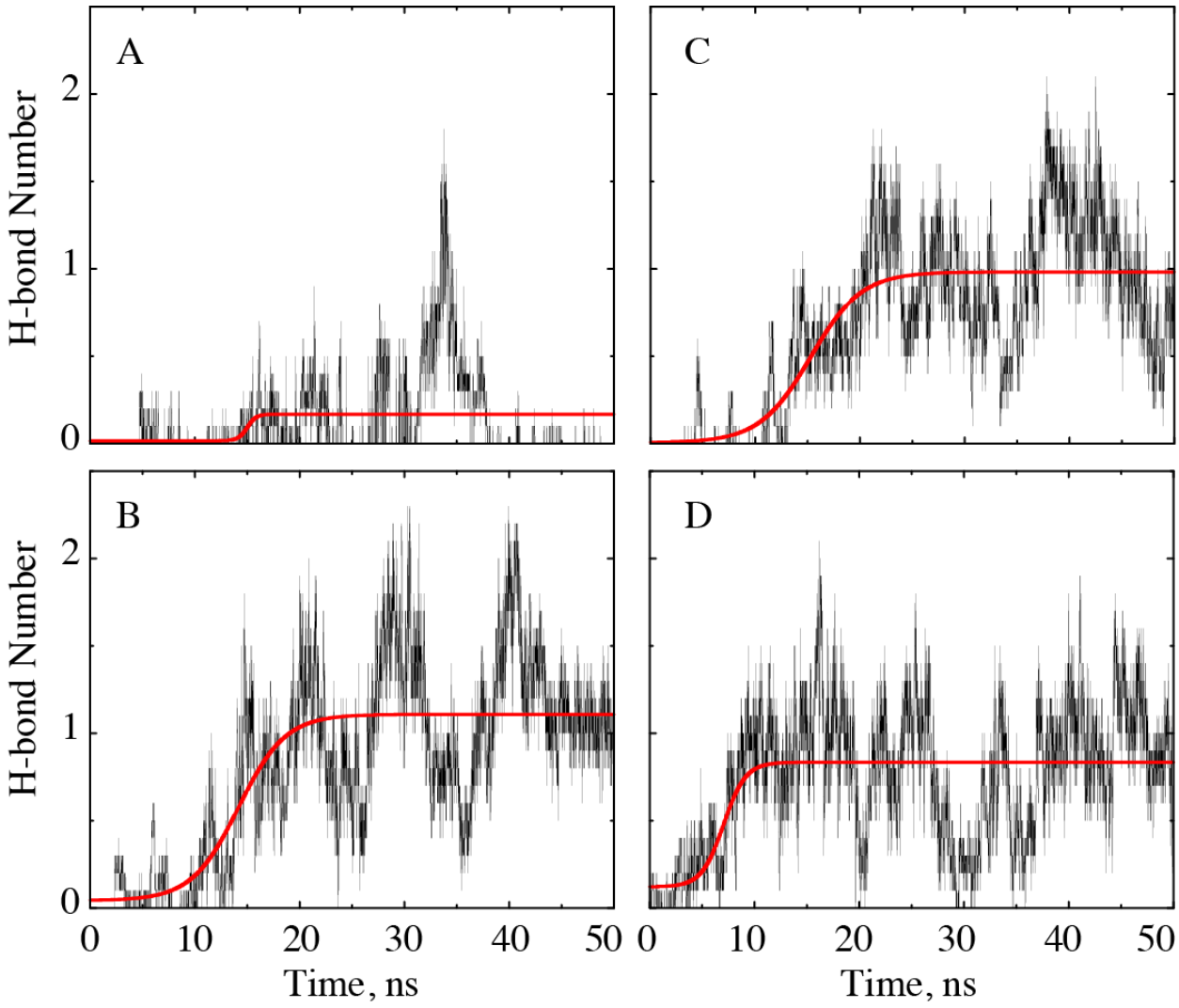

Figure S6. Time dependence of hydrogen bond number on time. The inter-chain backbone hydrogen bond number is plotted as a function of time for simulations of (A) hI2-Zn, (B) hI3-Zn, (C) hI4-Zn, and (D) hI6-Zn. The hydrogen bond number is averaged over 10 independent DMD simulations. The red lines correspond to the sigmoidal fitting using Eq. 1. The corresponding fitted values are listed in Table 1.

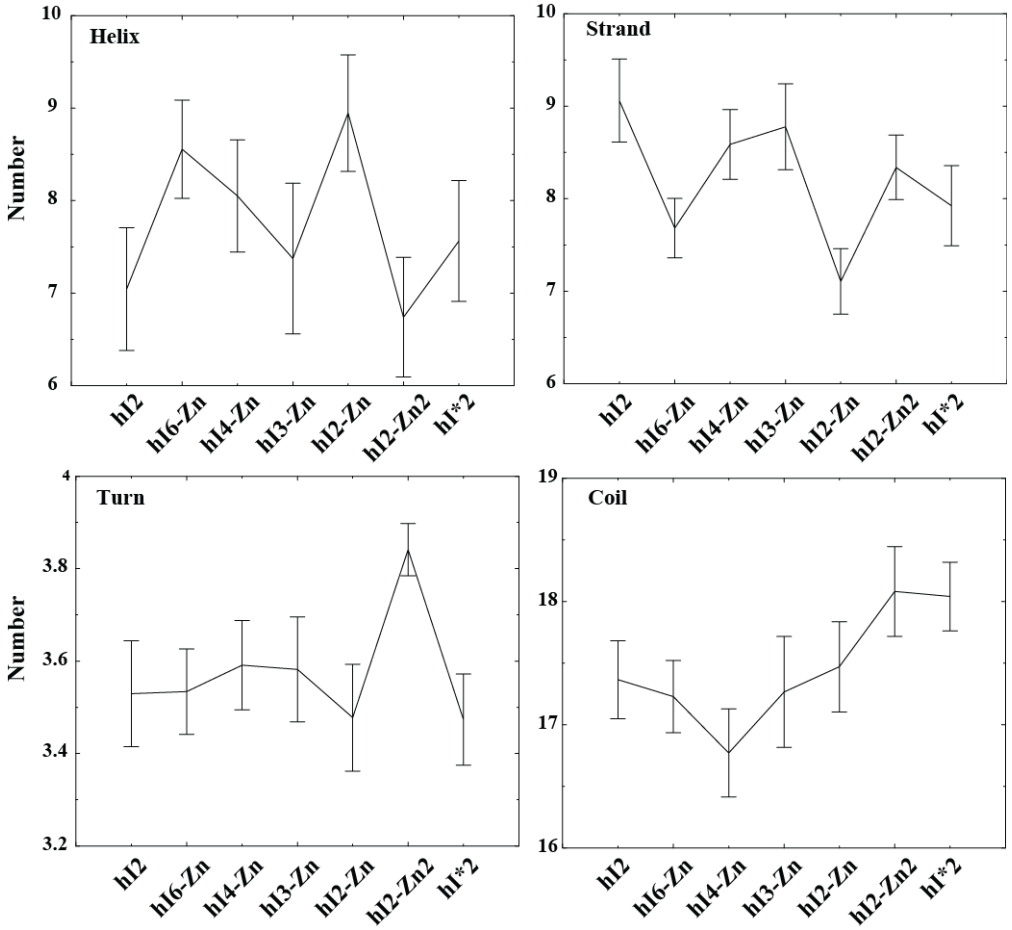

Figure S7. Secondary structure contents of different zinc-coordinated hIAPP oligomers. The total secondary structure contents (per chain) for different oligomers coordinated by zinc ion. Unlike the contact number, or local hydrogen bonds, secondary structure contents show no clear trend as a function of coordination number.